

COAL SLURRY pH STUDIES

Karl S. Vorres
Chemistry Div., Bldg. 211
Argonne National Laboratory
Argonne, IL 60439

ABSTRACT

Coal slurry pH values can be used to characterize coals. pH values depend on the coal, time since slurry preparation, contact with gas atmosphere, particle size, and stirring. Measured values reflect a sequence of reactions probably including: carbon dioxide absorption by water from the air, wetting of the coal (pH may be affected by the elemental composition of the mineral matter), and further equilibration with species in the water. The pH initially drops as carbon dioxide is absorbed, then rapidly increases as the coal is wetted, and then slowly decreases as some reactions with species in the water take place.

INTRODUCTION

Coal slurry pH values are used to characterize samples. It has been suggested as a means to indicate the degree of oxidation or weathering. The measurement procedure is similar to that used for soil samples (1). The usual procedure calls for the addition of a weighed quantity of coal and water (1:2), stirring well, and measurement of the pH of the liquid above the settled coal after a time period of one half hour.

The stirring is intended to quickly wet the hydrophobic coal particles so that they will be suspended in the slurry rather than remain on the surface of the mixture. The waiting period before the measurement implies a dynamic situation and an approach to a steady state pH value. This paper is intended to describe some of the changes which take place during the course of the period from the beginning of the mixing to several hours afterward. Several reactions are apparent from the changes which have been observed.

The wetting involves an interaction with the surface of the coal particles. The effect on pH includes at least dissolution of soluble acidic or basic species, interaction with surface acidic or basic functional groups, interaction with acidic or basic surface sites or areas. Oxidation can change the surface of the mineral as well as the organic parts of the coal, and can be expected to affect the pH. Some of these potential effects may be deduced from changes in the progression of pH with time for a sample.

EXPERIMENTAL

An Orion Model EA940 pH meter was used with an Accumet pH electrode. The electrode was calibrated with standard buffers of pH 4, 7 and 10. A two point method was used depending on the range of pH values involved in the experiment. Typically calibration was done at pH 7 and 10. Distilled and de-ionized water was used.

The coal samples were taken from the Argonne Premium Coal Sample Program set. Both -100 and -20 mesh samples were used. Water/coal ratios of 2-32 to 1 were obtained by mixing an ampule of 5 grams of -100 or 10 grams of -20 mesh coal with varying amounts of water. For some experiments a polyethylene plug (machined to fit inside the pyrex beaker and center the electrode in a snug-fitting hole) was used to limit the access to the atmosphere. For deaerated water experiments, the water was prepared by bubbling a stream of nitrogen through the stirred water for a minimum of 30 minutes. In one experiment, nitrogen gas was passed over the coal-containing equipment in a plastic enclosure. A magnetic stirrer was used in a number of experiments.

Sealed ampules were opened at the beginning of the experiment, weighed, water added and weighed, and mixed with a glass stirring rod or magnetic stirrer. Data were recorded on a IBM microcomputer at 15-20 second intervals. The computer data were analyzed using Lotus 123.

RESULTS AND DISCUSSION

A typical result for a Pittsburgh high volatile bituminous coal is shown in Figure 1. Initially the pH decreases as the water is stirred and affected by the atmosphere. As the coal is added the pH increases to a maximum value and then slowly decreases again. This general behavior pattern has been observed for most of the coal samples.

The initial decrease is believed to be due to the dissolution of carbon dioxide from the air, formation of carbonic acid, and ionization to provide hydronium and bicarbonate ions. The increase on addition of coal involves an interaction with the surface accessible to the water. This interaction consumes hydronium ions. The final slow decrease in pH may be again due to interaction with the carbon dioxide in the air.

The initial reaction with coal gives a series of maximum values. The value of the maximum does not correlate with carbon content or others of the organic elemental composition.

A series of runs with Illinois #6 (IL) indicated the effects of several values and produced a range of values for the maximum pH. For the -100 mesh samples run in pyrex beakers, the maxima were in the range 9.75-9.80. If a stainless steel beaker was used instead (250 ml) the maxima were in the pH range 9.65-9.71. These results were obtained over a water/coal ratio range of 2/1 to 32/1. However, for the -20 mesh sample with a water/coal ratio of 4, the pH range was lower, 9.61-9.76, with a value of 9.53 for the stainless steel beaker. The high values were obtained when the magnetic stirrer was off in the early stages of the run. Stirring introduced a limitation to the maximum pH, probably due to the incorporation of carbon dioxide from the atmosphere. Aerating or de-aerating the water had little effect on the maximum pH as both gave 9.72. Interestingly, a sample which had no gas bubbled through gave pH 9.67.

The run with equipment blanketed with nitrogen and de-aerated water gave the pH 9.76 which was higher than other stirred runs.

The effect of stirring speed was notable at low coal concentrations. Apparently, more rapid stirring gives a higher maximum pH.

In an effort to understand the reason for the increase in pH on the addition of coal to water, a series of materials were stirred with water. It was apparent that graphite did not behave like the coal, unless it was assumed that the behavior was like an extremely high rank coal. However the addition of titanium dioxide, as an example, gave a behavior very reminiscent of the plot of pH versus time for the coal samples. This observation would indicate that the pH may be due to the effect of various mineral constituents in the sample.

CONCLUSIONS

The measured pH value of a given coal slurry will depend on the parameters of the experiment, including water/coal ratio, stirring speed, particle size, and coal rank.

The addition of coal to water produces a series of pH changes. Initially, the drop in pH corresponds to the addition of carbon dioxide to the slurry. A subsequent increase appears to be related to inorganic constituents in the coal. A long term decrease in pH is assumed due to continued interaction with carbon dioxide.

The maximum pH depends on the interaction of the concentration of carbon dioxide, and the concentration of the mineral matter in the slurry.

ACKNOWLEDGMENT

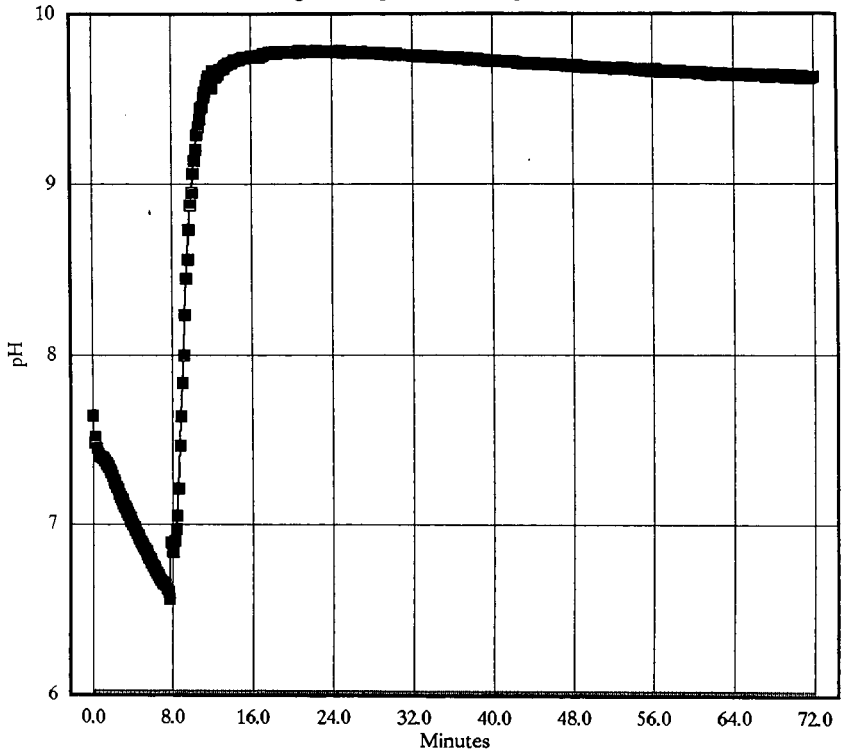
The author gratefully acknowledges the support of the U. S. Department of Energy, Office of Fossil Energy for financial support, and the staff at the Pittsburgh Energy Technology Center for help with this program.

REFERENCES

1. Methods of Soil Analysis, Part 2, Chemical and Microbiological Properties, ed. C. A. Black, Amer. Soc. of Agronomy, Madison, WI 1965, pp. 915-920.

Fig. 1, pH of PI-100 mesh Slurry

5 g coal, 35 g water in 50 ml pyrex beaker



PI922A94.wk3
ck

ADSORPTION ENTHALPIES FOR HYDROCARBONS ON WYODAK COAL SURFACES
BY INVERSE GAS CHROMATOGRAPHY

Amy S. Glass
Department of Chemistry
University of Dayton
Dayton, OH 45469-2357

(Keywords: Wyodak coal, coal surfaces, inverse gas chromatography)

Introduction

Studies of coal surface interactions are important for understanding how technologically important reagents interact with coal. Thermodynamic data provide a quantitative means to assess the interactions between reagents and coal. Knowledge of interaction strengths for solutes with coal surfaces should enable the design of more effective coal reaction strategies and lead to better utilization of coal as fuel and chemical feedstock.

In addition, studies of coal surface thermodynamics provide information about the structure and chemistry of coal. An important advantage with surface thermodynamic data is that they are not complicated by processes in bulk coal. For example, surface data are free of mass transport effects and intermolecular coal-coal associations which may exist in the bulk. Surface interaction data therefore provide a direct measure of the interaction between the solute and coal for a single specific type of chemical or physical property of the coal.

We recently developed the technique of inverse gas chromatography (IGC) for obtaining coal surface thermodynamics.¹ Solute molecules are carried past coal packed into a stainless steel tube. IGC provides a means to discriminate against the diffusion of solutes into bulk coal and thus enables the measurement of surface adsorption thermodynamics for polar and nonpolar molecules with coal surfaces. Coal IGC data are collected in the Henry's Law region of the adsorption isotherm, so the data represent interactions with the coal at infinite dilution surface coverage.

The present paper reports surface thermodynamic data for Wyodak coal surfaces. Because the coal is from the Argonne Premium Coal Sample Bank, it is intended that the interactions at this surface provide a benchmark for interactions of solutes with a low rank, high oxygen content coal. In the present work, it has been found that the Wyodak surface has relatively weak (low exothermicity) adsorption enthalpies with saturated hydrocarbons (alkanes) but quite strong (highly exothermic) interactions with alkenes and aromatic adsorbates. Recently, Ahsan et al. reported calorimetric data for aromatics with original and with citric acid washed (CAW) Wyodak coal.² These workers observed that citric acid washing of Wyodak coal caused heats of immersion (ΔH_{imm}) for the coal in aliphatic acids to decrease while ΔH_{imm} in aryl sulfonic acids increased. In contrast, CAW caused no changes in the ΔH_{imm} of Illinois No. 6 coal in these acids. Nishioka observed that alkylation or washing in 2N HCl caused a drastic increase in the swelling ratio of the pyridine insoluble portion of a Wyoming subbituminous coal.³ These changes were not observed for a higher rank Illinois No. 6 coal. He ascribed the changes in the Wyoming coal to the reduction of strong ionic forces in the coal by HCl or by the tetrabutyl ammonium salt which acts as a catalyst in the alkylation procedure. The existence of strong ionic forces in low rank coal is supported by the results of the present work. These forces make themselves felt in the unusually exothermic interactions of unsaturated hydrocarbon adsorbates with the Wyodak coal surface.

Theory

IGC differs from analytical GC in that in IGC the emphasis is on stationary phase properties as opposed to properties of the injected solute. In IGC, the retention volume serves as a measure

of the interaction strength between the single, pure injected solute and the stationary phase. The interaction is most straightforward in the regime of linear chromatography. In this regime, the retention volume represents the Henry's Law constant for the solute-stationary phase interaction. If the retention volume is sensitive to the surface of the stationary phase, then the Henry's Law constant expresses the equilibrium interaction between the injected solute and the stationary phase and gives the equilibrium constant for surface adsorption, K_s . This relationship is expressed by equation 1.

$$K_s = \frac{V_s}{RT} \quad (1)$$

where V_s is the retention volume per unit adsorbate gas pressure and per unit accessible surface area, S , of the stationary phase ($V_s = V_N/SRT$ where R is the ideal gas constant, T is the column temperature, and V_N is the retention volume corrected for pressure drop across the column.) The van't Hoff equation gives the enthalpy from the temperature dependence of the equilibrium constant. For equilibrium surface adsorption at infinite dilution surface coverage, the van't Hoff equation gives the isosteric adsorption enthalpy, q_{st} , as the slope of a plot of the natural logarithm of the retention volume over temperature vs. inverse temperature. Equation 2 is the defining equation:

$$\frac{d(\ln V_N/T)}{d(1/T)} = \frac{-q_{st}}{R} \quad (2)$$

Plots of $\ln(V_N/T)$ vs. $1/T$ were used to determine the isosteric adsorption enthalpies for saturated and unsaturated hydrocarbons on Wyodak coal surfaces.

Experimental

The procedure and apparatus for IGC of coal surfaces have been described previously.¹

Adsorbate liquids were obtained from Aldrich at the highest purities available and were used without further purification. They were admitted to the vacuum manifold for injection after at least 3 freeze-pump-thaw cycles. Adsorbate gases were obtained from Aldrich or from Matheson in the highest purities available and were admitted to the vacuum manifold directly. Wyodak coal (-20 mesh) was obtained from the Argonne Premium Coal Sample bank. The coal was sieved to 40/60 mesh and packed into 1/8 inch O.D. stainless steel tubes about 100 cm in length. The columns were heated in helium at 150°C or at 250°C for at least a week until the GC baseline stabilized. Significant weight loss (~30%) was observed. In order to eliminate the large dead volume these columns were repacked using coal which had been previously heated at 115°C in vacuum.

Retention volumes were determined from the first moments of the GC peaks. Van't Hoff plots were constructed using data obtained at temperature intervals of 5 to 10° over at least a 30° temperature range. At least 5 retention volumes were obtained at every temperature. The errors in the adsorption enthalpies were 7% or lower. Data for Illinois No. 6 coal are taken from reference 1.

Results and Discussion

Figure 1 shows plots of the isosteric adsorption heat, q_{st} , vs. the electronic volume polarizability of the adsorbates, α'_e , for *n*-alkane adsorbates on two different rank coals, an Illinois No. 6 bituminous coal and a Wyodak subbituminous coal.¹ Data for propene and 1-butene are also shown for the Illinois No. 6 coal. The lower plot is for alkanes on Wyodak coal and the upper plot is for alkanes on Illinois No. 6 coal. Both coals were heated at 150°C in helium. These plots demonstrate that these two coals have different dispersive surface interactions with alkanes. The Illinois No. 6 coal has more exothermic adsorption heats with alkanes, demonstrating that it has a more polarizable surface than

the Wyodak coal. Dispersive surface tensions, γ_s^d , have also been determined for the two coals, and are $\gamma_s^d=104 \text{ mJ/m}^2$ for Illinois No. 6 and $\gamma_s^d=25.2 \text{ mJ/m}^2$ for Wyodak.^{1,5} These data demonstrate that Wyodak coal possesses a relatively low energy surface, similar to those found for polymers such as polyethylene.⁶ This conclusion supports the idea that Wyodak coal has surface properties which are similar to those of its precursor, a polymeric cellulosic type of material. On the other hand, Illinois No. 6 coal possesses a higher energy surface, similar to those found for carbonaceous materials.⁴ As seen from the center plots, heating to 250°C or extracting either of the coals results in a surface with similar adsorption heats for alkanes. The adsorption heats for n-alkanes on both of these modified surfaces are similar to heats for alkanes on graphitized carbon black.⁴ The plot for Illinois No. 6 coal also shows data for two alkenes, propene and 1-butene. On Illinois No. 6 coal, alkene adsorbates have interactions which depend on adsorbate electronic polarizability (α') in the same way as the alkanes.

In Figure 2, adsorption heats for alkanes on Wyodak coal heated at 150°C and at 250°C are replotted. However, in Figure 2, these data are plotted vs. (total) volume polarizability, α' , whereas in Figure 1, they are plotted against electronic volume polarizability, α'_e . For alkanes, $\alpha'=\alpha'_e$, because these adsorbates only interact with the surface via induced dipole-induced dipole (London dispersion) forces. Also plotted in Figure 2 are adsorption heats for alkene and aromatic adsorbates on Wyodak coal. For alkenes, there is an additional induction contribution to α' . This contribution may make itself felt if there exists a dipole or Coulomb force at the surface which is capable of inducing a dipole in the adsorbate (Debye force).

Interpretation of the data for alkenes on the 250°C-heated coal appears relatively straightforward (Figure 2). The alkene adsorbates on this surface have q_s 's which depend on the total volume polarizability, α' , in the same way as the alkanes. (Alkenes on the 250°C-heated Wyodak surface have ~1.5-2.0 kcal/mol additional interaction with this surface over that expected from electronic polarizability (α'_e) alone.) Apparently, alkenes interact with this surface according to their total volume polarizabilities, α' . As seen from Figure 2, benzene has a somewhat stronger interaction with the 250°C-heated Wyodak coal surface than expected based on α' .

The data for alkenes on the 150°C-heated Wyodak surface appear to be more complex. (See Figure 2.) Propene and 1-butene have higher adsorption heats by ~3-4 kcal/mol with this surface than expected based on α' . It may be fortuitous that these adsorbates give adsorption heats on the 150°C-heated coal surface which equal those expected based on α' for the 250°C-heated coal surface.

Comparing the adsorption heats for alkenes on Illinois No. 6 coal (Figure 1) with those for alkenes on Wyodak coal (Figure 2) shows that there is an additional type of force operating at the Wyodak surface which produces more exothermic interactions with alkenes and aromatics. Ionic forces exist in low rank coals.³ At a surface, the presence of small cationic charges augments the adsorption heats with molecules that contain additional electron density in double, triple, or aromatic bonds.⁴ Such effects are observed for hydroxylated silica and for zeolite surfaces.⁴ Silica contains a cationic proton while zeolites contain Na^+ , Ca^{2+} , etc. ions. The existence of ionic forces at the Wyodak coal surface would explain the more exothermic adsorption heats with alkene and aromatic compared to alkane adsorbates. Studies are underway to explore the nature of these forces at the surfaces of original and modified Wyodak coal surfaces.

Acknowledgement

This work was supported by a Fellowship from the University of Dayton Research Council.

References

1. Glass, A. S.; Larsen, J. W. *Energy Fuels* 1994, 8, 629-636.
2. Ahsan, T.; Wu, J. H.; Arnett, E. M. *Fuel* 1994, 73, 417-422.
3. Nishioka, M. *Fuel* 1993, 72, 1725-1731.
4. Kiselev, A. V.; Yashin, Y. I. *Gas-Adsorption Chromatography*; Plenum: New York, 1969.
5. Glass, A. S., unpublished data.
6. Zisman, W. A. *Contact Angle, Wettability, and Adhesion*, ACS Adv. Chem. Ser. No. 43; American Chemical Society: Washington, DC, 1964; pp. 1-51.

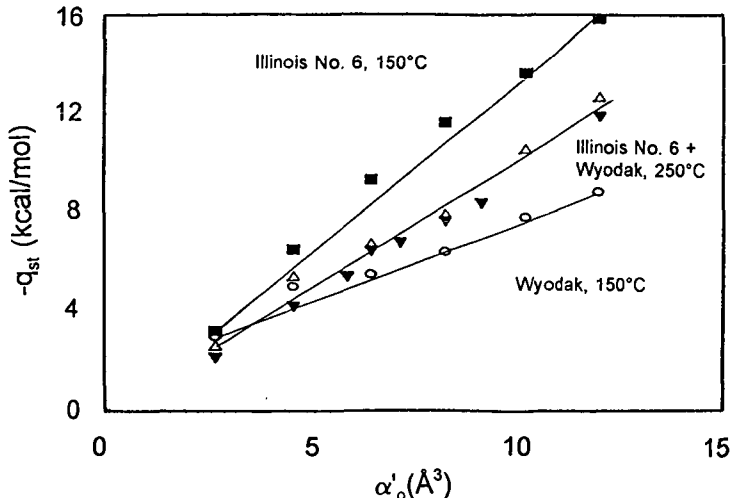


Figure 1. Isosteric adsorption heat (q_{st}) vs. electronic volume polarizability (α'_o) for hydrocarbons on Wyodak and Illinois No. 6 coal surfaces. ■=alkanes on Illinois No. 6 heated at 150°C. △=alkanes on Wyodak heated at 250°C. ○=alkanes on Wyodak heated at 150°C. For ■, △, ○ adsorbates are (from left to right): methane, ethane, propane, *n*-butane, *n*-pentane, *n*-hexane; ▽=alkanes and alkenes on Illinois No. 6 coal extracted in tetrahydrofuran and heated at 150°C. For ▽ adsorbates are: methane, ethane, cyclopropane, propane, propene, 1-butene, *n*-pentane, *n*-hexane. All coals heated in helium.

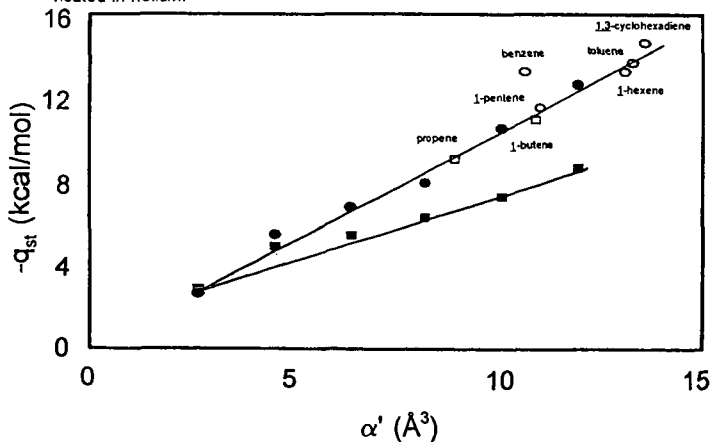


Figure 2. Isosteric adsorption heat (q_{st}) vs. volume polarizability (α') for hydrocarbons on Wyodak coal surfaces. ■=alkanes on Wyodak heated at 150°C. ●=alkanes on Wyodak heated at 250°C. □=alkenes on Wyodak heated at 150°C. ○=alkenes and aromatics on Wyodak heated at 250°C. For ■ and ● adsorbates are: methane, ethane, propane, *n*-butane, *n*-pentane, *n*-hexane. For □ adsorbates are propene and 1-butene. For ○ adsorbates are 1-pentene, 1-hexene, 1,3-cyclohexadiene, benzene, and toluene.

AIR OXIDATION-INDUCED EFFECT ON THE PYROLYSIS BEHAVIOR OF A SUBBITUMINOUS COAL FROM SOUTHERN ALASKA

Olayinka I. Ogunsola and Michael Downing
Mineral Industry Research Laboratory
School of Mineral Engineering
University of Alaska Fairbanks
Fairbanks, Alaska 99775-7240

Keywords: Alaskan low-rank coals; TGA; oxidation

ABSTRACT

A subbituminous coal from Beluga coalfield, Alaska was oxidized in air at 120°C for about 8 days. The pyrolysis behavior of the raw coal and oxidized samples was determined using a Perkin-Elmer Series 4 thermogravimetric analyzer (TGA). The TGA pyrolysis behavior of partially demineralized raw and oxidized samples was also conducted to investigate any accompanying effect of demineralization. Results obtained indicate a decrease in the maximum decomposition rate and apparent reactivity and an increase in activation energy of devolatilization of the coal when it was air oxidized. The effect was found to be less significant in the demineralized coal.

INTRODUCTION

The complex and heterogeneous nature of coal has made understanding of its structure very difficult. Oxidation is one of the methods of evaluating the physical and chemical structural properties of coal. Considerable emphasis has been placed on oxidation as a means of understanding coal chemistry[1]. Efforts have also been made to conduct studies in order to address some practical implications of oxidation on coking and agglomerating potentials[2] and ignition, and spontaneous combustion characteristics of coal[3-5].

Many studies have been conducted on coal oxidation, review of which has been given in the literature[6-8]. From these previous studies, impact of oxidation on the coal properties that are of practical significance to coal beneficiation and utilization has been established. For example, chemical changes that occur during coal oxidation affect flotation behavior of stockpiled run of mine coal and the coking potential of the stockpiled products[9].

In addition to the effect of atmospheric oxidation of coal on its properties, beneficiation, quality and utilization, coal oxidation in a stream of air has been used to enhance production of humic acids, which are used as fertilizers, from coal[3,10-13]. The materials produced during atmospheric coal oxidation depends on the rank, type, and nature of the coal and on the oxidation conditions (e.g. temperature and period of oxidation)[10,13]. While studies have been conducted on the production of humic acid from oxidized British coal[3], Spanish coals[10], European brown coals[12], and Alaskan coals[13], no study has been conducted to address the effect of atmosphere oxidation on the pyrolysis behavior of Alaskan coals. The effects of thermal upgrading on the performance of an interior Alaska low-rank coal during pyrolysis (an important stage of coal utilization processes) have only been recently studied[14]. About half of the U.S. coals are located in the state of Alaska[15]. Alaskan coals, which are estimated at about 5.5 trillion tons[15], are of Cretaceous and Tertiary age[16] and are mainly of low rank[17].

This paper discusses the results of a preliminary study on the effect of air oxidation and demineralization on the devolatilization behavior of Beluga subbituminous coal using thermogravimetric analysis (TGA) technique. Decomposition characteristics and reactivity of oxidized and unoxidized coal samples were obtained.

EXPERIMENTAL

The coal sample used in this investigation was a subbituminous C coal from Beluga field, west of Anchorage, Alaska. Analytical characteristics of the coal are summarized in Table 1.

The bulk coal sample was collected in lump size from the mine and taken to the laboratory in plastic bag contained in steel metal container under nitrogen. The coal sample was crushed to pass through 60 mesh. The minus 325 mesh size fraction was sieved off. The 60 x 325 mesh fraction was split into 4. One split of the sample was partially demineralized, one split was oxidized while another split of each sample was used for the analytical characterization.

Prior to oxidation, one split of the sample was partially demineralized according to the method used by Estevez, et al.[10]. This was achieved by suspending the coal in 0.5N HCl (1:10 w/v) for one hour at ambient temperature with continuous mechanical stirring. The partial demineralization was done in order to evaluate the catalytic effect (if any) of the mineral matter on oxidation[10].

The demineralized and undemineralized coal samples were oxidized at a temperature of 120°C for a period of about eight days in an air forced circulation oven. The pyrolysis behavior of the raw and oxidized coal samples was investigated using a Perkin-Elmer TGS-4 thermogravimetric analyzer. About 5 mg sample was scanned from 350°C to 950°C at a rate of 20°C/min. under nitrogen gas flowing at a rate of 80 cc/min. A series of runs was conducted before the actual runs to obtain the best conditions for excellent reproducibility. Reproducibility was best at the experimental conditions used. Sample was purged for about 15 minutes in nitrogen prior to run.

Thermograms and differential thermograms of the samples were obtained from which data, such as decomposition regions, pyrolysis rate, activation energy and thermal reactivity, were obtained and/or calculated.

RESULTS AND DISCUSSION

Figure 1 shows the thermograms/differential thermograms (TG/DTG) for the raw Beluga coal used in this study. Two distinct weight loss regions, one at about 119°C and the other at about 343°C can be observed for the unoxidized coal. Corresponding TG/DTG curves were obtained for the oxidized demineralized (BDX8) sample and the oxidized undemineralized sample. Table 2 shows the rate of weight loss at the two regions and the temperature at which they occur for the feed and treated samples. The first weight loss region, which is attributed to loss of moisture, occurred at a slightly lower temperature for the oxidized coal than the raw coal. Partial demineralization appears to reduce the extent of decrease in the temperature at which the first region occurs as shown by the results on Table 2. The second weight loss region, which indicates onset of primary decomposition and entails primary devolatilization, occurred at 343°C for the raw coal and at 329°C and 331°C, respectively for the undemineralized oxidized and demineralized oxidized samples. Also, shown on Table 2 is the maximum devolatilization rate which occurred at the second region. It could be observed from the results on Table 2 that oxidation of the Beluga coal decreased its maximum decomposition rate from about 0.181 mg/hr/mg to about 0.156 mg/hr/mg. The maximum devolatilization rate of the coal was only decreased to 0.17 mg/hr/mg when the coal was demineralized prior to oxidation. Although the decomposition kinetics of coal are very complex [18-19], some useful kinetic information such as the activation energy was obtained. Apparent activation energies of decomposition over 475°C - 800°C temperature range were obtained for the raw and treated coal samples from the Arrhenius equation plotted in Figure 2, for the raw coal, oxidized coal, and oxidized demineralized coal, on the assumption that thermal decomposition was a first order that followed the relationship:

$$-dw/dt = kw \quad (1)$$

where dw/dt = instantaneous rate of weight loss, w = undecomposed decomposable matter, and k = specific reaction rate. The reaction rate was then related to the Arrhenius equation by

$$\ln k = \ln A - E_a/RT \quad (2)$$

where A = the frequency factor, R = the universal gas constant, E_a = activation energy and T = absolute temperature.

Values of k were obtained at various temperatures by using data from TG and DTG curves. The apparent activation energies for the raw coal and the oxidized undemineralized and oxidized demineralized samples were determined from plots of $\ln k$ versus $1/T$, shown in Figures 2. The activation energy of the coal was increased by about 50% from 16.9 KJ/mol to about 26 KJ/mol when it was oxidized for eight days as depicted by the results on Table 2. Little or no change in activation energy was observed when the coal was demineralized prior to oxidation. Apparent activation energy of the raw coal in this study appears to be lower than those reported by others [19] for other coals of similar rank. However, activation energy of thermal decomposition of coal has been reported to be as low as 20 KJ/mol [20]. Maximum decomposition rate has been related to thermal reactivity of coal [19, 21-23]. From a kinetic view point the maximum decomposition rate is related to the reactivity R by

$$R = 1/w_i (dw/dt)_{\max} \quad (3)$$

where w_i = initial weight of coal (mg) and $(dw/dt)_{\max}$ = maximum loss rate (mg/min).

Table 2 gives the value of reactivity for the raw coal and treated samples. A slight decrease in the reactivity of the coal could be observed when the coal was demineralized and oxidized for eight days. A more significant decrease in the reactivity occurred when the coal was not demineralized prior to oxidation as illustrated on Table 2.

CONCLUSIONS

The thermal reactivity and apparent activation energy of the Alaskan subbituminous C coal have been found to be affected by oxidation in air at a temperature of 120°C. A decrease in reactivity and a corresponding increase in apparent activation energy have been observed when the coal was oxidized for eight days. Demineralizing the coal prior to oxidation was found to reduce the effect of oxidation on both thermal reactivity and apparent activation energy.

REFERENCES

1. Elliott, M.A. in 'Chemistry of Coal Utilization', John Wiley & Sons, New York, USA, 1981, p. 455-460.
2. Kalema, W.S. and Gavalas, G.R. *Fuel* 1987, 66, 158.
3. Swartz, D., Hall, P.J. and Marsh, H., *Fuel* 68, 1989, 868.
4. Painter, P.C., Snyder, R.W., Pearson, D.E. and Kwong, J., *Fuels* 1980, 59, 282.
5. Liotta, R., Brown, G. and Isaacs, J. *Fuels* 63, 1984, 935.
6. Berkowitz, N. "An Introduction to Coal Technology," Academic Press, New York, 1979, p. 96.
7. Andersen, N.F. and Hamza, H.A., "The Characterization of Oxidized Coal-A Review," Proc. CIC Symp., Halifax, Nova Scotia, 1981, p. 117.

8. Barkowitz, N., "Atmospheric Oxidation of Coal," in Sampling, Selection, Aging, and Reactivity of Coal, (Klein, ed.), John Wiley and Sons Inc., New York, 1989, pp. 217-289.
9. Mikula, R.J., Axelson, D.E., and Michaelian, K.H., "Oxidation and Weathering of Stockpiled Western Canadian Coals," CANMET Divisional Report ERP/CRL 85-105(OP-3), 1985.
10. Estevez, M., Juan, R., Ruiz, C. and Andres, J.M. Fuel 69, 1990, 57.
11. Juan, R., Ruiz, C., Andres, J.M. and Estevez, M., Fuel 69, 1990, 61.
12. Unarov, T., Zh., Pobedonostseva, O.I. and Pobedorostseva, N.I., Solid Fuel Chem. 15(4), 1981, 35.
13. Ogunsola, O.I. and Rao, P.D., Fuel 72, 1992, p. 1121.
14. Ogunsola, O.I. and Rao, P.D., "Effect of Thermal Treatment on the Pyrolysis Behavior of Alaskan Low-Rank Coals," Proc. Ninth Annual Int. Pittsburgh Coal Conference, Pittsburgh, p. 509, 1992.
15. Merritt, R.D. and Hawley, C.C., "Map of Alaska's Coal Resources," Alaska DNR Special Report 37, 1986.
16. Youtcheff, J.S., "Characterization of Alaskan Coals-Evaluation of their Liquefaction Behavior," MIRC Report No. 72, p. 366, 1986.
17. Rao, P.D., Walsh, D.E., Willson, W., and Li, Yu-Fu, "Characterization of Hydrothermally and Evaporatively Dried Coals and Char Products from Usibelli Subbituminous C Coals," Paper Presented at the Low Rank Fuel Symposium, Billings, Montana, May 20-23, 1991.
18. Kasperski, K.H. and Ogunsola, O.I., Thermal Analysis of Nigerian Coals Using Thermogravimetry, Presented at the 24th Annual Conf. of Canadian Institute of Chemical Engineers, Halifax, Nova Scotia (1989).
19. Cummings, J.W., Reactivity Assessment of Coals Using a Weighted Mean Activation Energy, Fuel 63 (1984), 1436.
20. Anthony, D.B. and Howard, J.B., Coal Devolatilization and Hydrogasification, AIChE J. 27 (1976), 625.
21. Jenkins, R.G., Nandi, S.P. and Walker, P.L., Jr., Reactivity of Heated Treated Coals in Air at 500°C, Fuel 52 (1975), 288.
22. Mahajan, O.P. and Walker, P.L., Jr., Reactivity of Heat Treated Coals, in C. Karr (Ed.), Analytical Methods for Coal and Coal Products Vol. II, Academic Press, Inc., 1978, pp. 465-494.
23. Leslie, I.H., Jost, M., and Kruger, C.H., Measured and Predicted Char Reactivity of Three U.S. Coals, Combustion and Flames 78 (1989), 195.

TABLE 1. Characteristics of Beluga coal

<u>Beluga Coal</u>	
Proximate analysis: (wt%, ASTM equilibrium moisture basis)	
Moisture	24.40
Ash	7.71
Volatile matter	33.72
Fixed carbon	34.18
Ultimate analysis: (wt%, ASTM equilibrium moisture basis)	
Carbon	46.73
Hydrogen	6.88
Nitrogen	0.71
Sulfur	0.18
Oxygen	37.79
Heating Value (MJ/kg)	18.84

TABLE 2. Summary of Results

	Raw Coal BxO	Oxidized Coal for 8 days, Bx8	Oxidized demineralized coal for 8 days, Bdx8
Peak Temperature of Region 1, (°C)	119	110	113
Peak Temperature of Region 2, (°C)	343	329	331
Weight Loss Rate at Region 1, (Mg/Min)	0.028	0.022	0.019
Weight Loss Rate at Region 2, (Mg/Min)	0.181	0.156	0.170
Maximum Decomposition Rate, (Mg/Min)	0.181	0.156	0.170
Temperature of max. dw/dt, (°C)	343	329	331
Apparent Reactivity, daf, (Mg/hr/mg)	2.43	1.98	2.06
Activation Energy, (KJ/mol *k)	16.90	25.98	16.7

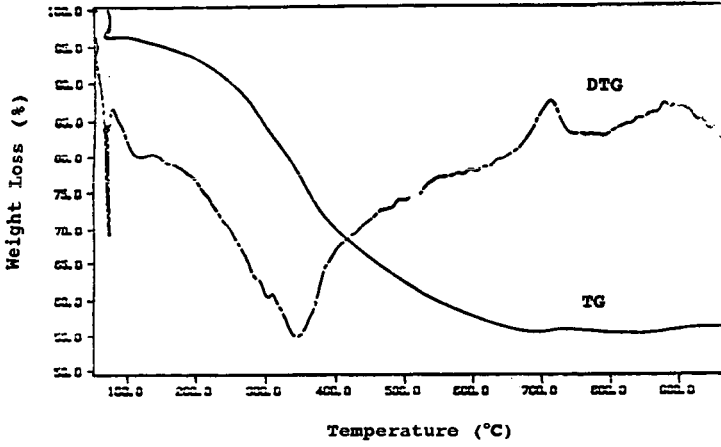


Figure 1. Thermograph of Raw Coal

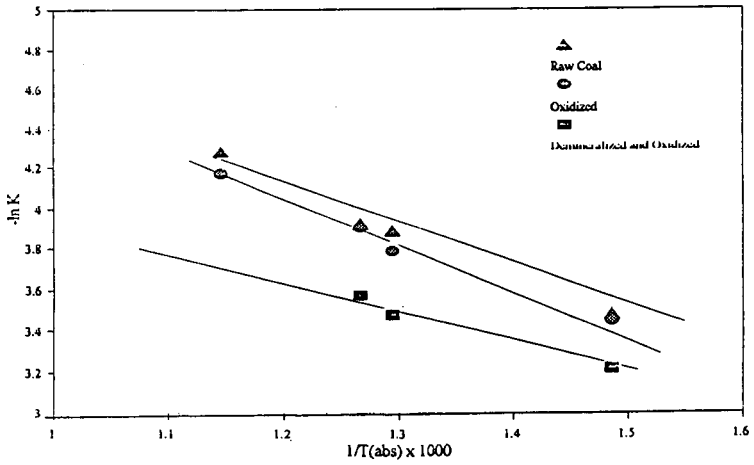


Figure 2. $-\ln K$ versus $1/T$ (abs. $\times 1000$)

P.S. Virk and V.J. Vlastnik
 Department of Chemical Engineering
 M. I. T., Cambridge, MA 02139

KEYWORDS: Thermolysis, Reaction Paths, Kinetics, Demethylation, Hydrogen Transfer.

INTRODUCTION

Motivation. This work on thermolysis of 9-methyl-anthracene, abbr 9MA, is a part of our continuing studies of methylated acenes, that mimic the chemical moieties found in complex fossil materials of engineering interest. Also, since 9MA is a primary product of 9,10-dimethyl-anthracene, abbr 910DMA, thermolysis [1, 2], it was hoped that information regarding the former might buttress our understanding [3] of 910DMA thermolyses at high conversions.

Previous Work. The earliest work we could find on 9MA thermolysis was by Pomerantz [4], who reported its half-life to be ~ 25000 s at $T = 400$ C for an initial concentration $[9MA]_0 \sim 0.15$ mol/l, with anthracene, abbr ANT, as the major product, accompanied by lesser amounts of 1- and 2-methyl-anthracenes, abbr 1MA, 2MA, and 9,10-dihydro-anthracene, abbr DHA. Subsequently, in a brief experimental and mechanistic study of 910DMA thermolysis at $310 < T < 390$, conducted in the present authors' laboratory, Pope [5] pointed out that 9MA can give rise to two delocalized radicals,



 HMA9* and HMA10*, of which only the latter can propagate the demethylation pathway to ANT. Most recently, Smith & Savage [6] have pyrolysed 9MA at $350 < T < 400$ using $[9MA]_0 \sim 0.09$ mol/l. Their decomposition kinetics were ~ 20 -fold faster than those reported by Pomerantz [4] and they detected dimethyl-anthracenes, abbr DMAs, among the products, in addition to the ANT, 1MA, 2MA and DHA previously found.

Outline. We first describe the experiments and present results for the concentration histories, product selectivities, and kinetics observed during 9MA thermolysis. Reaction pathways for the decomposition of 9MA are then inferred from the major products observed, and their ratios. Finally, a free-radical mechanism comprising 22 elementary steps is proposed for 9MA thermolysis at low conversions, and shown to accommodate many of the experimental observations.

EXPERIMENTAL

Conditions. Table 1 summarizes conditions for, and results obtained from, the present experiments. The first column of this table refers to 9MA substrate and its second to 910DMA, the latter serving as a basis for later comparisons. The upper portion of Table 1 summarizes conditions for the experiments, listing the model substrates, their structures and the ranges of temperatures, holding times and initial concentrations studied, as well as the temperatures at which light gases were analysed. Thermolyses were conducted in batch reactors, volume 0.6 ml, made from 1/4" stainless steel Swagelok parts. The reactors were charged with weighed amounts of biphenyl (internal standard) and substrate (9MA) totalling 0.30 g, sealed and placed in an isothermal, fluidized-sand bath for the appropriate holding times, after which they were quenched in ice-water, and their contents extracted into methylene chloride. Reactor contents were in the liquid phase during all experiments.

Assays. Gaseous and liquid thermolysis products were identified and analyzed by GC, augmented by GC/MS. All gas peaks were identified by injections of standards. Most liquid products were identified by injections of standards with some minor liquid products identified by determining their masses by GC/MS and relating their retention times to those of known molecules. Heavy thermolysis products, mostly dehydrogenated dimers of the substrates, were identified by GC/MS. For example, in 9MA thermolyses, the MS of a prominent late GC peak showed a molecular ion at mass 382 and a fragment at mass 191, suggestive of a bibenzylidene, dehydrogenated dimer of 9MA called 9MAD. Product assay trains developed for 9MA substrate using the preceding GC and GC/MS techniques typically identified ~ 15 reaction products. Identified products accounted for $> 70\%$ of the reacted mass at substrate fractional conversions $0.2 < X < 0.8$. Experimental details are available [7].

RESULTS and DISCUSSION

Histories. Fig. 1 chronicles the concentration histories of substrate and products during thermolysis of 9MA at $T = 370$ C and $[C]_0 = 0.82$ mol/l, using arithmetic coordinates of absolute mols J of either substrate or product present in the reactor versus reaction holding time t in seconds. Part (a), upper panel, shows that the substrate 9MA decayed monotonically, with half-life $t^* \sim 23000$ s. The products formed, in order of their abundance, were ANT, various dimethyl-anthracenes, abbr ALL DMAs, methane CH₄, 1MA, 2MA, and trimethyl-anthracenes, abbr TMA. Part (b), lower panel, details histories of the individually identified dimethyl-anthracene isomers and several 9,10 dihydro- species. The DMAs include 9,10-DMA (major), and 1,10-, 1,9-, and 2,9- + 3,9-DMA, while the hydrogenated species are DHMA (major), DHDMA, and DHA. The formation of DMAs and DHMA products concurrent with ANT shows that during 9MA thermolysis, methylation and hydrogenation always occur in parallel with demethylation. It is also interesting that the isomers 1MA and 2MA both arose subsequent to ANT, which suggests that they formed from methylation of ANT rather than from the isomerization of 9MA.

Selectivities. Fig. 2 depicts the preceding product history data as selectivity diagrams, with ordinate of product selectivity $S = \text{mols J produced/mol of substrate 910DMA decomposed}$, and abscissa of substrate fractional conversion X . Parts (a), upper panel, and (b), lower panel, show that the products formed at low conversions, $X < 0.30$, were ANT, DMAs, DHMA, and CH_4 with selectivities respectively $S = 0.30, 0.20, \sim 0.10$ and 0.05 . With increasing conversions, to $X \sim 0.60$, the selectivity to ANT increased somewhat, to $S \sim 0.35$; the DMAs showed a shallow maximum, $S \sim 0.20$ at $X \sim 0.4$ and then declined slightly; DHMA declined sharply, to $S \sim 0.03$ at $X \sim 0.6$, and CH_4 increased monotonically, to $S \sim 0.15$ at $X \sim 0.6$. The sum of the selectivities of all identified liquid products (squares) was ~ 0.75 over the major range of conversions, $0.2 < X < 0.6$, from which the selectivity of unidentified, mostly heavy, product formation is inferred to be ~ -0.25 .

Kinetics. 9MA decomposition kinetics are illustrated in Fig. 3. Part (a), upper panel, is a log-log plot of decay half-life t^* versus initial concentration $[9\text{MA}]_0$ at fixed temperature. The data, spanning 1.5 decades of $[9\text{MA}]_0$, describe a line of slope $-1/2$, which implies that the decomposition was of 3/2 order wrt substrate. Part (b), bottom panel, is an Arrhenius type of semi-log plot, showing decay half-life t^* versus the reciprocal of a scaled absolute temperature $\Theta = 0.004573^*(T\text{ C} + 273.2)$. Here the data span almost two decades of t^* and lie on a line of slope ~ -46 , which latter is directly the activation energy of decomposition E^* , kcal/mol. The observed kinetics are summarized in Table 1, which shows decay half-lives at $T = 370\text{ C}$, orders wrt substrate, and Arrhenius parameters ($\log A, E^*$). Both the decompositions of 9MA and of 910DMA are of 3/2 order wrt the substrate and exhibit activation energies ~ 45 kcal/mol; their relative decomposition rates are roughly in the ratio 1 : 2.

Product Ratios. The importance of each of the observed hydrogenation, methylation, and methane formation pathways relative to the dominant demethylation pathway can be assessed from the respective primary product ratios R , namely $R[\text{DHMA}/\text{ANT}]$, $R[\text{DMAs}/\text{ANT}]$ and $R[\text{CH}_4/\text{ANT}]$. Of these, the ratio of hydrogenation to demethylation $R[\text{DHMA}/\text{ANT}] \rightarrow 0.7$ at the lowest conversions, $X \rightarrow 0$, and then decreased rapidly to 0.05 ± 0.025 for $0.20 < X < 0.75$; this variation of $R[\text{DHMA}/\text{ANT}]$ versus X was essentially independent of initial concentration and temperature. Fig. 4(a), left panel, shows that the ratio of methylation to demethylation $R[\text{DMAs}/\text{ANT}] \sim 0.8 \pm 0.1$ for $X < 0.3$ at all temperatures while Fig. 4(b), right panel, shows that the ratio of methane formation to demethylation $R[\text{CH}_4/\text{ANT}] = 0.20 \pm 0.03$ for $X < 0.3$ at $T = 370\text{ C}$. The sum $R[\text{DMAs}/\text{ANT}] + R[\text{CH}_4/\text{ANT}] \sim 1.0$ was close to unity, accounting for the methyl radicals implicitly associated with the demethylation pathway. Thus, at low substrate conversions, $\sim 1/5$ of all methyl radicals formed were quenched by hydrogen abstraction, forming methane gas, while $\sim 4/5$ were trapped by addition to the 9MA substrate, eventually appearing as DMAs. These results for 9MA substrate are in striking contrast to those for 910DMA [3], wherein $\sim 3/4$ of methyl radicals were quenched by hydrogen abstraction while $\sim 1/4$ were trapped by addition to the substrate. Since 9MA and 910DMA respectively possess 3 and 6 benzylic H-atoms per molecule, the observed [H-abstraction/addition] ratios of $1/4$ versus $3/1$ show the methyl addition affinity of 9MA to be 6-fold greater than that of 910DMA. The greater methyl affinity of 9MA relative to 910DMA likely derives from the potency of its unsubstituted 10-position as an addition site.

Pathways. The foregoing observations lead to the 9MA decomposition pathways depicted in Fig. 5. Three primary pathways operate in parallel: (P1) Hydrogenation, to DHMA, (P2) Demethylation, to ANT, and (P3) Methylation, to 910DMA. Too, the demethylated acene product is associated with formation of methane gas CH_4 , and the scheme also includes formation of a heavy bibenzylidic dimer of 9MA called 9MAD. Further, the primary demethylation and methylation products shown in the above scheme can be secondarily operated upon by a pathway triad analogous to the one from which they arose, leading, recursively, to the formation of a variety of methylated and hydrogenated acenes. This is evident in the appearance, at high conversions, of TMAs, a host of DMAs, 1MA and 2MA, as well as DHA and DHDMA (for clarity, these secondary products were omitted from Fig. 5). Pathway results are summarized in the bottom of Table 1, which shows major product selectivities and ratios at $T = 370\text{ C}$ and conversions $X = 0.05$ and 0.4 . Results for 9MA were akin to those obtained for 910DMA, but showed a two-fold greater selectivity to the methylated product, and also roughly two-fold greater ratios of hydrogenated/demethylated and of methylated/demethylated products at low conversions.

Mechanism. A possible mechanism for 9MA thermolysis is presented in Fig. 6, an elementary step "graph" constructed with substrate and all stable molecular products arrayed in the bottom row and unstable radical intermediates arrayed in the top row. Reaction "nodes", in the middle row, connect the individual species in the bottom and top rows with arrows indicating the initial direction of reaction (all reactions are reversible). Initiation reactions are denoted by solid interconnecting lines, propagation reactions by dashed lines and termination reactions by dotted lines. The 9MA substrate is in the middle of the bottom row, with light (propagation) products to its right and heavy (termination) products to its left. Consider first a subset of the full mechanism comprising reactions (R1-R10). This free-radical cycle is initiated by the bimolecular disproportionation of substrate (R1), an intermolecular hydrogen transfer reaction, to form the respectively dehydrogenated and hydrogenated radical species 9MA^* and $\text{HMA}10^*$. Of these, the latter can either abstract hydrogen from 9MA by (R2), to form DHMA product, or undergo a β -scission type of radical decomposition by (R3), forming ANT product and a methyl radical CH_3^* . The CH_3^* can either abstract H from 9MA by (R4), to form methane product, or add to 9MA by (R5), to form the dimethyl radical HDMA^* . The latter can then abstract H from 9MA via (R6) to form the observed 910DMA product. The cycle is terminated by the species 9MA^* and $\text{HMA}10^*$ engaging in both pure- and cross-combinations, (R7-R9), to form various dimeric products. $\text{HMA}10^*$

radical can also terminate by disproportionation, (R10), to form 9MA and DHMA. The foregoing portion of the full 9MA mechanism is evidently analogous to the 910DMA mechanism devised earlier [2, 3]. However, the 9MA substrate permits formation of an additional radical, HMA9*, which can engage in all the steps shown for HMA10* except for C-C bond scission, giving rise to steps (R11-R22) of the full mechanism. Thus substrate disproportionation by (R11) forms 9MA* and HMA9*, of which the latter can abstract hydrogen from 9MA by (R12), to form DHMA product. HMA9* can also form from H-transfer reactions (R16), between HDMA* and 9MA, and (R17), between HMA10* and 9MA, the latter causing radical isomerization. Finally, HMA9* can engage in a variety of termination reactions, including pure- and cross-combinations (R18, R19, R21) that form dimeric products, and disproportionations (R20, R22) that form 9MA and DHMA.

The proposed mechanism accounts for the major products, ANT, DMAs, DHMA, CH4 and heavies, observed during the initial stages of 9MA thermolysis. Each of the observed triad of primary pathways, namely, P1 hydrogenation, P2 demethylation and P3 methylation, also arise naturally as limiting cases of the elementary step graph, with P1 comprising the sets [R1, R2, R7] and [R11, R12, R7], P2 the set [R1, R3, R4, R7] and P3 the set [R1, R3, R5, R6, R7]. The stoichiometry of these sets restricts the maximum selectivity of each major product to 1/3, which is of the magnitude of the highest selectivities actually observed. The mechanism also offers some theoretical insights. It suggests that the relative kinetics of hydrogenation to demethylation, (P1)/(P2), are controlled by the HMA9* and HMA10* radicals. The HMA10* radical propagates both hydrogenation (R2) and demethylation (R3), but HMA9* propagates only hydrogenation (R12). It follows that the pathway ratio (P1)/(P2) = [(R2)+(R12)]/(R3) for 9MA should exceed that for 910DMA, which has only a single radical carrier analogous to HMA10*. This accords with the observations in Table 1, which show (P1)/(P2) for 9MA almost twice that for 910DMA at low X. Further, the methylation to demethylation ratio, (P3)/(P2), is essentially governed by competition between methyl radical reactions (R4) and (R5), in which CH₃* either abstracts H from or adds to the 9MA substrate. In this regard, H-abstraction from 9MA should be less favoured than that from 910DMA by a statistical factor of 2, but 9MA possesses a potent unsubstituted 10-position in addition to all the unsubstituted positions present in 910DMA, so methyl radical addition to 9MA should be greatly favoured over that to 910DMA. Theoretically, therefore, the pathway ratio (P3)/(P2) for 9MA should exceed that for 910DMA. This accords with observations in Table 1 which show (P3)/(P2) for 9MA from 1.5 to 2 times that for 910DMA over the entire range of substrate conversions.

In future work it is hoped that the mechanism presented above will provide a basis for the further quantitative modelling and numerical simulation of 9MA and 910DMA thermolyses.

ACKNOWLEDGEMENT: This work was supported in part by Cabot Corporation, Boston, MA.

REFERENCES

- [1] Virk, P.S.; Vlastnik, V.J.: PREPRINTS, Div. of Fuel Chem., ACS, **37**(2), 947 (1992).
- [2] Virk, P.S.; Vlastnik, V.J.: PREPRINTS, Div. of Petrol. Chem., ACS, **28**(2), 422 (1993).
- [3] Virk, P.S.; Vlastnik, V.J.: PREPRINTS, Div. of Fuel Chem., ACS, **32**(2), 546 (1994).
- [4] Pomerantz, M.; Combs Jr., G.L.; Fink, R.: J. Org. Chem., **45**, 143 (1980).
- [5] Pope, J.M.: Ph.D. Thesis, Dept. of Chem. Eng., MIT, Cambridge, MA (1987).
- [6] Smith, C.M.; Savage, P.E.: A.I.Ch.E. J., **39**, 1355 (1993).
- [7] Vlastnik, V.J.: Sc.D. Thesis, Dept. of Chem. Eng., MIT, Cambridge, MA (1993).

Table 1. Experimental Grid, Kinetics, and Major Product Selectivities and Ratios for Thermolyses of 9MA and 910DMA.

Substrate Structure	9MA	910DMA	
			
Experimental Grid			
Temperature, T C	315-409	315-409	
Holding Time, t s	450-57600	450-57600	
Initial Concentration, [C] ₀ , mol/l	0.082-2.06	0.082-2.47	
Gas Analyses at T C	370	335, 370	
Kinetics			
Decay Half-Life, t* s at T = 370 C	23000	9900	
Order wrt substrate	1.50	1.53	
Arrhenius Parameters (log A, E*)	(11.4, 46.4)	(10.6, 43.1)	
Product Selectivities at T = 370 C	X		
Demethylated	0.4	0.37	0.42
Methylated	0.4	0.22	0.10
Hydrogenated	0.05	0.03	0.06
Heavies	0.4	0.13	0.15
Product Ratios at T = 370 C	X		
[Hydrogenated/Demethylated]	0.05	0.43	0.21
	0.4	0.05	0.04
[Methylated/Demethylated]	0.05	0.69	0.35
	0.4	0.59	0.24

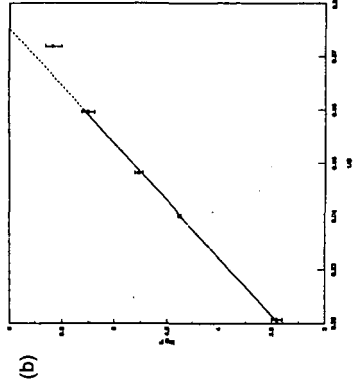
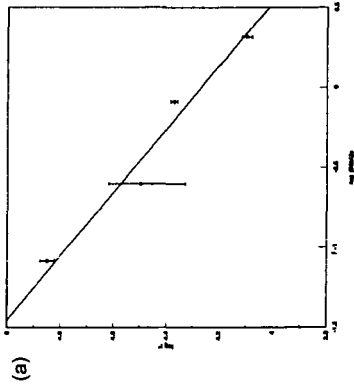


Fig. 3. 9MA thermolysis kinetics.
 (a) Effect of $[9MA]_0$ at fixed $T = 370$ C.
 (b) Arrhenius diagram for fixed $[9MA]_0 = 0.82$ mol/l.

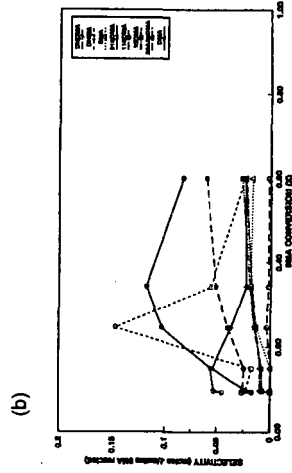
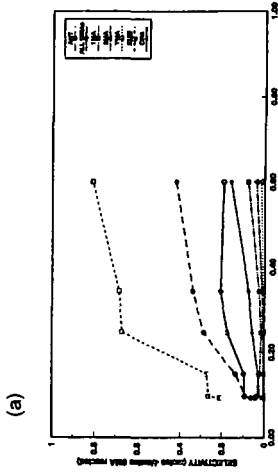


Fig. 2. Product selectivities for 9MA thermolysis at $T = 370$ C, $[9MA]_0 = 0.82$ mol/l.
 (a) ANT, DMAS, 1MA, 2MA, TMA, SUM, CH4.
 (b) All other products.

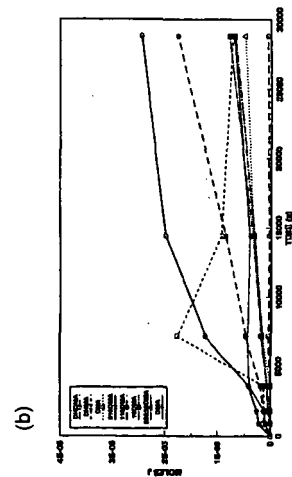
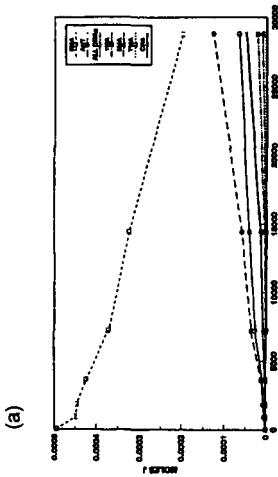


Fig. 1. Substrate and product histories for 9MA thermolysis at $T = 370$ C, $[9MA]_0 = 0.82$ mol/l.
 (a) 9MA, ANT, DMAS, 1MA, 2MA, TMA, CH4.
 (b) All other products.

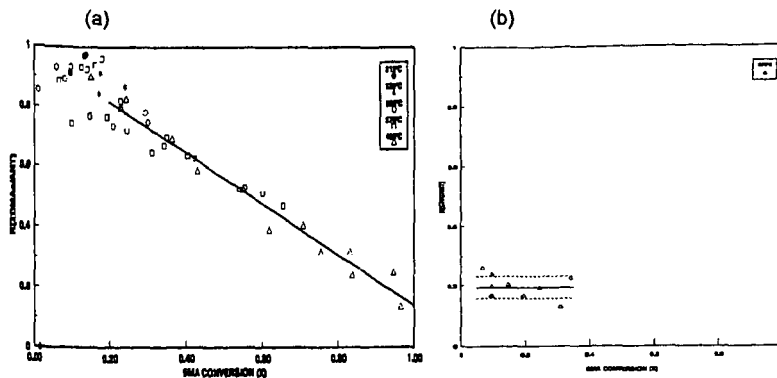


Fig. 4. Major product ratios in 9MA Thermolyses.
 (a) $R[\text{DMA}/\text{ANT}]$ at $T = 315$ to 409 C and $[\text{9MA}]_0 = 0.82$ mol/l.
 (b) $R[\text{CH}_4/\text{ANT}]$ at $T = 370$ C and $[\text{9MA}]_0 = 0.82$ mol/l.

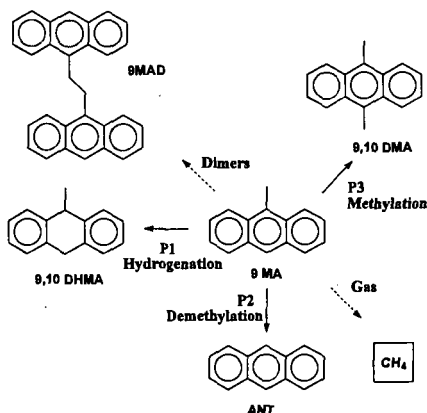


Fig. 5. Major pathways in 9MA thermolysis.

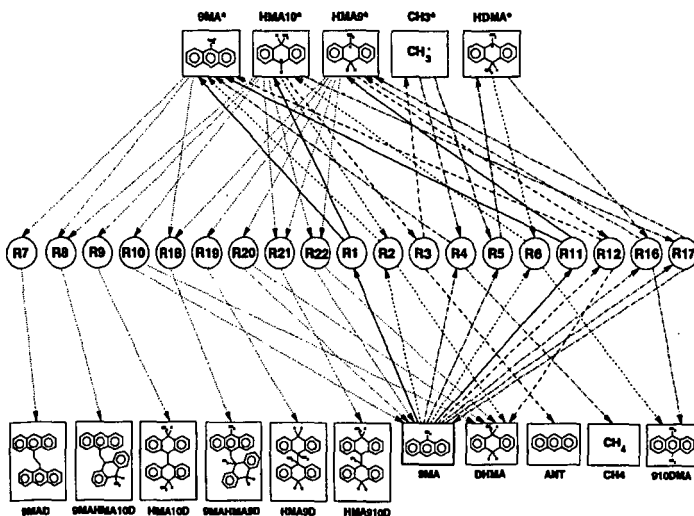


Fig. 6. Elementary step graph of 9MA thermolysis mechanism at low conversions.

CONVERSION OF WASTE POLYVINYL CHLORIDE (PVC) TO USEFUL CHEMICALS

T. Kamo, Y. Yamamoto, K. Miki, Y. Sato
National Institute for Resources and Environment
16-3, Onogawa, Tsukuba-shi, Ibaraki, 305, Japan

Keywords: PVC, Recycling, Pyrolysis, Liquefaction

INTRODUCTION

Developments of recycling technologies are expected one of the most important keys for saving energy and resources, and minimization impact for environment. For instance, combustion of waste for power generation and conversion of plastics into liquid fuels have been studying for thermal energy recycling ^{1), 2)}. However, PVC has been excepted from the most of these experiments. Because, heat of combustion of PVC is almost a half of other plastics', hydrogen chloride, which is produced at low temperature, corrodes the combustion chamber, and PVC causes coking reaction during pyrolysis of plastics.

Numerous investigations have been conducted on degradation of PVC. However, most of these experiments were done to improve heat resistance of PVC ^{3),4)} or to study reaction mechanism of PVC degradation ^{5),6)}. Pyrolysis of PVC into liquid products have been studying since 1960's from a view of environmental protection ^{7),8),9)}. Recently, Y. Maezawa et al. reported PVC was converted into oil at 600 °C with sodium hydroxide ¹⁰⁾. However, more than 50 % of hydrocarbon fraction of PVC was converted to residue and gas in their experiment. We are going to develop a new technology to convert of PVC into useful chemicals or liquid fuels at high efficiency by using hydrogen donor solvent.

In this experiment, we used PVC resin, because commercial PVC contain many other compounds as stabilizer. Chlorine in PVC was removed by pretreatment to prevent corrosion of an autoclave. We liquefied pretreated PVC resin in tetralin with some catalysts.

EXPERIMENTAL

Pre treatment of PVC: PVC resin was supplied Mitsubishi Kasei Vinyl Company. The PVC resin (100 g) was charged in a Pyrex flask (300 ml) and heated with nitrogen gas flowing. The samples were heated according to following temperature program, 200 °C (24 hours), 250 °C (24 hours) and 300 °C (24 hours). Finally, the samples were heated at 300 °C for 24 hours under vacuum. Weight of samples decreased less than 40 % of initial PVC resin after the pre treatment. Elemental analyses of original PVC resin and pretreated PVC resin were shown in Table 1. The pretreated resin still contained 2.8 % of chlorine.

Reaction procedure: Pretreated PVC resin (10.0 g) and tetralin (70.0 g) were charged into a 300 ml magnetic stirred autoclave. In order to study effects of catalysts on product distribution and content of remained chlorine in products, nickel - molybdenum catalyst for upgrading of petroleum (NiMo/Al₂O₃, 1.0 g) and sulfur (0.5 g), iron oxide (Fe₂O₃, 1.0g) and sulfur (0.5 g), Zeolite for FCC (1.0 g), and fine nickel powder (Ni, 1.0 g, diameter < 0.3 μm) were added in a few experiments. All reactions were carried out at 440 °C and 470 °C under an initial pressure of 6.9 MPa of hydrogen gas or nitrogen gas. Reaction products were separated residues and liquid products by filtration. The liquid products were vacuum distilled at 330 °C for 60 min. The vacuum bottoms were separated HS (hexane soluble) and HI (hexane insoluble) by hexane extraction. The residue and extracted products, HS and HI, were dried for one day at 110 °C under vacuum and weighted.

Analysis of products: Gas products were collected into a Teflon bag through 10% of sodium hydroxide aqueous solution and analyzed by gas chromatography (GASUKURO KOGYO, GC-312, molecular sieve 5A, molecular sieve 13X, Porapak N, gasukuro 54, and VZ-7). Liquid products were analyzed by gas chromatography (CARLO ERBA INSTRUMENTS, HRGC 5300) with capillary column (HP Ultra 1, 0.2 mm, 50m). Chlorine content in product was measured by total chlorine analyzer (Mitsubishi Kasei, TOX-10Σ).

RESULTS AND DISCUSSION

Product distributions from the pretreated PVC resins were shown Figure 1. Yields of each product were obtained by using an equation shown below. Oil yields were calculated from yields of gas, HS, HI and residue.

$$\text{yield}(i) = \frac{\text{weight of product (i)}}{\text{weight of hydrocarbon fraction in chlorine removed PVC}} \times 100$$

Yields of gas and residue were only 3 % and 13 % respectively at 440°C under nitrogen gas. Y. Maezawa et al.¹⁰ reported that more than 50 % of hydrocarbon fraction in PVC was converted to gas and residue under conventional pyrolysis condition with sodium hydroxide. Remarkable decreases of yields of gas and residue observed in our experiment were caused by using hydrogen donor solvent. Product distribution from pretreated PVC indicates that hydrogen gas and NiMo/Al₂O₃ catalyst enhanced conversion of HS to oil and residue to HI at 440 °C. However, decomposition of HI to HS was not promoted in spite of presence of hydrogen gas and NiMo/Al₂O₃ catalyst. Yields of oil and HS increased with temperature significantly. Oil yield and HS yield were achieved to 40 % and 44 % respectively at 470 °C with NiMo/Al₂O₃ under hydrogen gas.

Methane, ethane, propane were produced mainly under our reaction condition. Production of methane increased particularly at 470 °C. Benzene, toluene and xylene (BTX) were produced as main liquid products from the pretreated PVC. Total yields of BTX were shown in Figure 2. Yields of these products increased with temperature significantly under hydrogen gas. These trends imply hydrogen gas enhanced production of BTX from pretreated PVC. Tetralin isomer, alkylated tetralin and tetralin dimer were observed in the solvent after liquefaction. Productions of these compounds indicate hydrogen was transferred from tetralin very rapidly, isomerization and dimerization of tetralin radical were enhanced.

In order to show effects of various catalysts on pyrolysis of pretreated PVC, NiMo/Al₂O₃, iron oxide (Fe₂O₃), Zeolite and fine nickel powder were used. Product distributions of these catalysts were shown in Figure 3. Remarkable increases of oil yield or HS yield were not observed at 440°C. The NiMo/Al₂O₃ was most effective catalyst for pyrolysis of pretreated PVC.

Low chlorine contents of products are very important to use them as chemicals and liquid fuels. Chlorine contents of products from liquefaction were shown Figure 4. Chlorine contents of oil and vacuum bottom (HI+HS) were 25 ppm and 8 ppm respectively under nitrogen gas at 440 °C. These results show 99.9% of chlorine in pretreated PVC was removed by liquefaction. Chlorine contents of oil and HS+HI produced under hydrogen gas were lower than that of products obtained under nitrogen gas. Under hydrogen gas with NiMo/Al₂O₃, chlorine content of oil and HS+HI were only 2 ppm and 3 ppm respectively. Remarkable decreases of chlorine content were observed at 470 °C. Chlorine content decreased with severity of hydrogenation of products. These results imply chlorine was removed by hydrogenation reaction of products.

Effects of catalysts on chlorine content of HS+HI were shown in Figure 5. Iron oxide and fine nickel powder did not show remarkable effects on removal of

chlorine in products. On the other hand, zeolite inhibited removal of chlorine from products. This negative effect was estimated to be caused by strong acidity of zeolite.

SUMMARY AND CONCLUSION

PVC was heated under nitrogen gas to remove chlorine at 300 °C for 24 hours. Then, pretreated PVC was liquefied in tetralin at 440 °C and 470 °C for 60 minutes under an initial pressure of 6.9 MPa of hydrogen gas and nitrogen gas. Oil yield and HS yield were 40 % and 44 % respectively at 470 °C with NiMo/Al₂O₃ under hydrogen gas. Benzene, toluene and xylene were produced as main liquid product. Chlorine content in products decreased with temperature. Less than 3 ppm of chlorine was retained in oil and vacuum bottom (HS+HI) at 470 °C under hydrogen gas with NiMo/Al₂O₃. Hydrogen transferred from tetralin and hydrogen gas enhance conversion of pretreated PVC to liquid products and removal of chlorine from products.

ACKNOWLEDGMENTS

We greatly thank T. Ueda, Japan PVC Association and H. Yamamoto, Mitsubishi Kasei Vinyl Company for supply PVC resin. We also acknowledge T. Imagawa, National Institute for Resources and Environment, Hydrosphere Environmental Protection Dept. for use of the total chlorine analyzer.

REFERENCE

- 1) D. S. Scott, S. R. Czernik, J. Piskorz and D. St. A. G. Radlein, *Energy & Fuels*, 4, 407 (1990).
- 2) R. C. Bailie, *Combustion*, 2, 13 (1974).
- 3) A. H. Frye and R. W. Horst, *J. Polym. Sci.*, 40, 419 (1959).
- 4) N. Bensemra, T. Van. Hoang, A. Guyot, M. Gay and L. Garette, *Poly., Deg. & Stab.*, 24, 89 (1989).
- 5) V. H. Tran, C. Carrigues, T. P. Nguyen and P. Molinie, *Poly. Deg. & Stab.*, 42, 189 (1993).
- 6) M. Rogstedt, and T. Hjertberg, *Macromolecules*, 25, 6332, (1992).
- 7) K. Saito and A. Kishi, Ichihashi, *The 2nd Japan Symposium on Thermophysical Properties*, 23 (1981).
- 8) Z. Mayer and J. Macromol. Sci., *Revs. Macromol. Chem.*, C10(2), 263 (1974).
- 9) S. Matsuzawa, T. Abe, H. Ando, O. Inomata and Y. Shimizu, *Bulletin of The National Research Institute for Pollution and Resources*, 4(1), 33 (1974).
- 10) Y. Maezawa, F. Tezuka, Y. Inoue, *Toshiba Review*, 49(1), 39 (1994).

Table 1 Elemental analyses of PVC and pretreated PVC

	C	H	O	Cl	H/C	O/C	Cl/C
PVC (resin)	38.64	4.81		56.53 ¹⁾	1.48		0.50
Pretreated PVC (300°C)	85.99	7.10		2.84	0.98		0.01

1) calculated (100 - C% - H%)

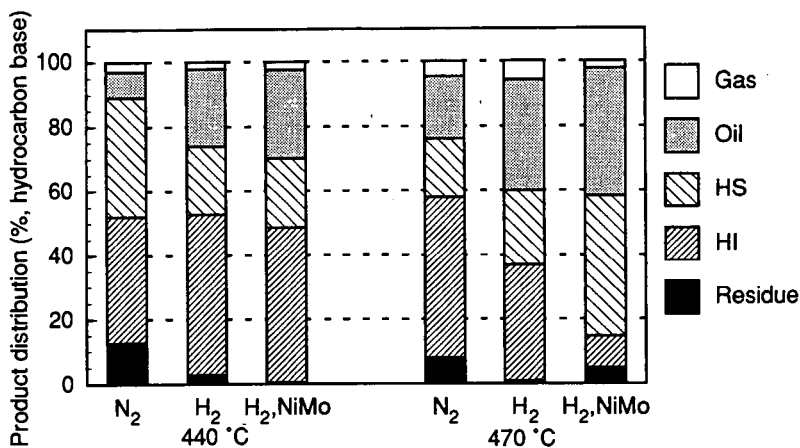


Figure 1 Distribution of products from pretreated PVC.

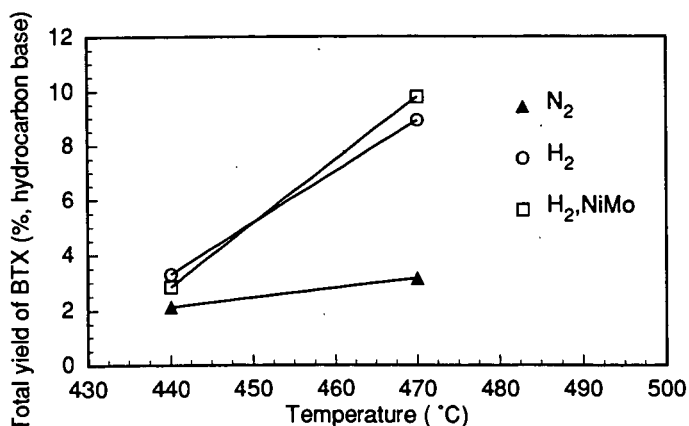


Figure 2 Total yield of benzene, toluene and xylene from pretreated PVC.

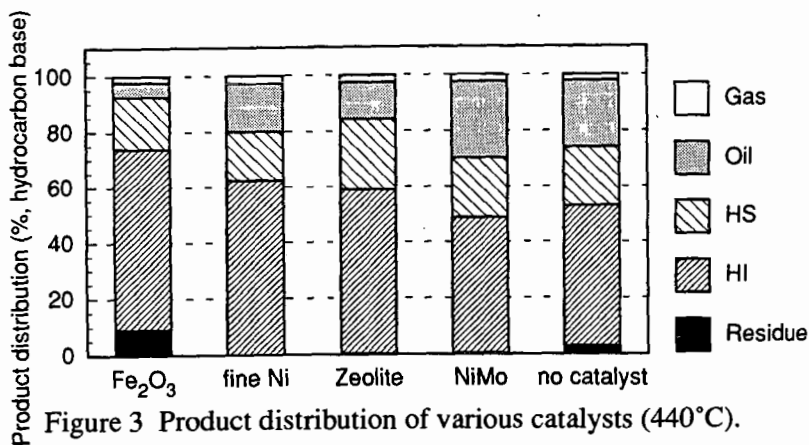


Figure 3 Product distribution of various catalysts (440°C).

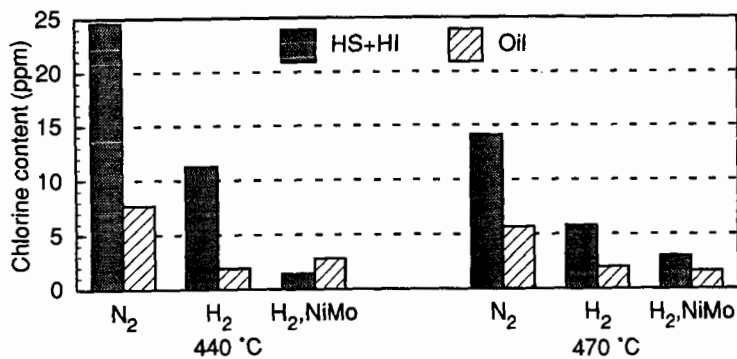


Figure 4 Chlorine content of oil and vacuum bottom (HS+HI).

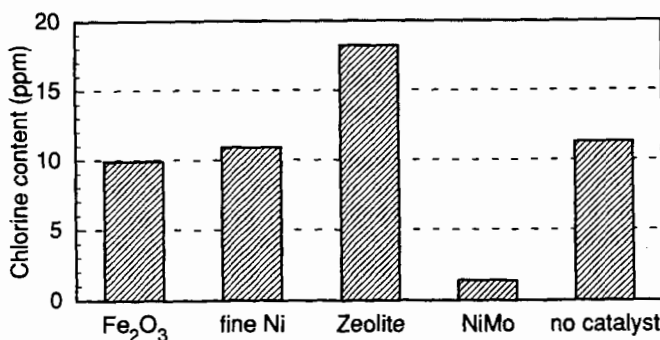


Figure 5 Effect of catalysts on chlorine content of vacuum bottom (HS + HI).